Supplementary Information

Double selective ionic gel with excellent thermopower and ultra-high energy density for low-quality thermal energy harvesting

Jindong Hu, Jiuyang Wei, Jinming Li, Long Bai*, Yang Liu*, Zhiguo Li*

Key Laboratory of Bio-based Material Science and Technology of Ministry of Education, College of Material Science and Engineering, Northeast Forestry University, Harbin 150040, P.R. China

***E-mail:**

Zhiguo Li: lizgmse@nefu.edu.cn

Yang Liu: liuyang@nefu.edu.cn

Long Bai: long.bai@nefu.edu.cn

Supplementary note

Thermopower of ITECs

In this section, the synergistic contribution of thermodiffusion and thermogalvanic effect was derived.[1]

Thermodiffusive thermopower

The thermodiffusive thermopower is defined as:

$$Std = -\frac{V(Th) - V(Tc)}{\Delta T} \qquad (S1)$$

where $V(Th)$ and $V(Tc)$ represent the voltage at the hot temperature Th and cold temperature Tc, respectively. Different from electronic semiconductive TE material, the sign of Std in an ionic system is determined by the type of charge with higher thermal mobility in the solution. Therefore, the transportation of ions under a temperature gradient, which is also known as the Soret effect, should be the key point to determine the thermopower of the ionic system.

Onsager's theory for irreversible processes provides a good framework for understanding of the ion's motions. In a system with two current flows (heat and mass) and each of them can be driven by the other, the current of each flow can be expressed by Onsager's theory, where the current J of the solute species (or ions) can be expressed as:

$$J = -L_{ii}\frac{1}{T}\nabla\mu - L_{iq}\frac{1}{T^2}\nabla q \qquad (S2)$$

where the first term describes Fick diffusion (or mass diffusion) with coefficient Lii and the second one describes the thermodiffusion with the Onsager cross coefficient Liq. Different from simple chemical ssystems the potential term μ in this system consists of both chemical potential and electrical potential, which can be regarded as the electrochemical potential. The coefficient

Lii, Liq can be obtained from experiments and theories. After the illustration and simplifications, the thermopower of the ionic system can be expressed as:

$$St\ \ d\hat{=}\frac{n_{+}D_{+}\hat{S}_{+}-n_{-}D_{-}\hat{S}_{-}}{e\ n(_{+}D_{+}+n_{-}D_{-})}\qquad S3\ \ )\qquad\qquad ($$

where $\hat{S}$ is charge of the electron, n is the concentration of the ion, D is the mass diffusion coefficient, is Eastman entropy of transfer and the sign "+" and "–" represents the cations and anions, respectively. Similar to the Einstein's relation for diffusion driven by a concentration gradient, the diffusion driven by temperature gradient can also have a thermal mobility which is defined as $D\hat{S}/k_BT$. The Eastman entropy of transfer is directly related to the heat of transport Q*, which has dependence on the size of ions and dielectric constant of the solutes by Born theory. For asymmetric electrolytes such as $FeCl_3/FeCl_2$ ($2n+ = n-$ or $3n+ = n-$ in this system most of the Fe^{3+} is adsorbed, so we choose $2n+ = n-$), Eq. 3 can be simplified as: [2]

$$St\ \ d\hat{=}\frac{D_{+}\hat{S}_{+}-2D_{-}\hat{S}_{-}}{e\ D(_{+}+2D_{-})}\qquad S4\ \ )\qquad\qquad ($$

From Eq. 4, without electric field and concentration gradient, the thermally driven ionic flux is simply $J_i=-n_i\frac{D_i\hat{S}_i}{k_BT}\nabla T$. If we relate ionic flux to "thermodiffusion velocity v_i^Tthrough $J_i=-n_iv_i^T$, then the relation between thermodiffusion velocity and the temperature gradient $-\nabla T$ is derived as $v_i^T=\frac{D_i\hat{S}_i}{k_BT}(-\nabla T)$. Therefore, we can define the thermal mobility μ_i^T:

$$\mu_i^T=\frac{D_i\hat{S}_i}{k_BT}\qquad S5\ \ )\qquad\qquad ($$

Eq. S5 is essentially the Einstein's relation for thermodiffusion. With the ionic mobility defined as $\mu_i^I = \frac{D_i}{k_B T}$, Eastman entropy of transfer is essentially the ratio between thermal mobility and ionic mobility. Further, charge mobility of ions is defined as:

$$\mu_i^q = \frac{q_i D_i}{k_B T} \qquad (S6)$$

Eq. S4 can be further re-written in a simpler form:

$$S_t^* = \frac{\mu_+^T - 2\mu_-^T}{\mu_+^q + 2\mu_-^q} \qquad (S7)$$

Therefore, we can see that the difference in thermal mobilities of the cations and anions determines the sign of the thermopower, and the thermal mobility is simultaneously determined by diffusion coefficient D and the Eastman entropy of transfer S^*.

Thermogalvanic thermopower[3]

The thermopower for a ITECs is an entropically driven process, and the corresponding thermopower S_{tg} is defined as follows:

$$S_{tg} = \frac{\Delta E}{\Delta T} = \frac{\Delta S}{nF} \qquad (S8)$$

where ΔE is the open-circuit voltage, n is the number of the electrons transferred in the redox reaction, F is the Faraday's constant and ΔS is the entropy difference for the redox reaction.

For some redox reactions (aA + ne ↔ bB). The redox effects of these systems are concentration dependent and their Stg can be estimated using the Nernst equation. The equilibrium potential E can be expressed as:

$$E = E^0 + \frac{RT}{nF} \ln \frac{(\alpha_A)^a}{(\alpha_B)^b} \qquad (S9)$$

where E^0 is the standard potential, α_A and α_B are the activities of the oxidation and reduction species, respectively, and R is the ideal gas constant. The activity α and concentration C are related by $\alpha = C \times \gamma$, where γ is the activity coefficient. Thus, Eq. S9 can be expressed as follows:

$$E = E^0 + \frac{RT}{nF}\left[\ln\frac{(\gamma_A)^a}{(\gamma_B)^b} + \ln\frac{(C_A)^a}{(C_B)^b}\right] \qquad (S10)$$

The thermopower S_{tg} can be expressed as follows:

$$S_{tg} = -\frac{E_h - E_c}{T_h - T_c} \qquad (S11)$$

where E_h and E_c are the potentials at the hot and cold electrodes, respectively. By substituting Eq. S10 into Eq. S11, we obtain the following equation:

$$S_{tg} = -\frac{E_h^0 - E_c^0}{T_h - T_c} - \frac{R}{nF\Delta T}\left[T_H\ln\frac{(\gamma_A)_H{}^a}{(\gamma_B)_H{}^b} - T_c\ln\frac{(\gamma_A)_C{}^a}{(\gamma_B)_C{}^b}\right] - \frac{R}{nF\Delta T}\left[T_H\ln\frac{(C_A)_H{}^a}{(C_B)_H{}^b} - T_c\ln\frac{(C_A)_C{}^a}{(C_B)_C{}^b}\right] \qquad (S12)$$

In electrochemistry, the temperature coefficient α_R is defined as:

$$\alpha_R = \frac{E_h^0 - E_c^0}{T_h - T_c} \qquad (S13)$$

The α_R can be further related to the entropy change of the redox reaction as follows:

$$\alpha_R = \frac{S_{red} - S_{ox}}{nF} = \frac{\Delta S}{nF} \qquad (S14)$$

where S_{red} and S_{ox} are the partial molar entropies of the reduced and oxidized states, and ΔS is the partial molar entropy change. Substituting Eq. S13 and Eq. S14 into Eq. S12, we obtain

$$S_{tg} = -\frac{\Delta S}{nF}\frac{R}{nF\Delta T}\left[T_H\ln\frac{(\gamma_A)_H{}^a}{(\gamma_B)_H{}^b} - T_c\ln\frac{(\gamma_A)_C{}^a}{(\gamma_B)_C{}^b}\right] - \frac{R}{nF\Delta T}\left[T_H\ln\frac{(C_A)_H{}^a}{(C_B)_H{}^b} - T_c\ln\frac{(C_A)_C{}^a}{(C_B)_C{}^b}\right] \qquad (S15)$$

The first term on the right-hand side of Eq. S15 is the intrinsic entropy change of the occurring reaction of the redox electrolyte, the second term is related to the entropy change of redox substances induced by other activities, e.g., the phase change of selective

complexation/dissociation of CG-$MA_{4\%}$ and Fe^{3+}, and the third term is related to concentration difference of redox substances between two electrodes.

Coupling between thermodiffusion and thermogalvanic effect

The total thermopower can be written as the sum of the different ionic species S_i:

$$S_i = S_{tg} + S_{td}(Fe^{3+/2+} - Cl^-) + S_{td}(Chitosan) \quad (S16)$$

where S_{tg} is the thermopower contributed by the thermogalvanic effect, $S_{td}(Fe^{3+/2+}\text{-}Cl^-)$ is the thermopower contributed by the thermodiffusion effect, and $S_{td}(Chitosan)$ is the thermopower contributed by the thermodiffusion effect of chitosan gel. According to **Fig. S19**, the S_{td}(Chitosan), $S_{td}(Fe^{3+/2+}\text{-}Cl^-)$, S_{tg} is -1.15, -2.39, and -3.69 mV K^{-1}, respectively, contributing 15.9%, 33.06%, and 51.04% to the thermopower of CG-$MA_{4\%}$, respectively.

Supplementary figures and disucssions

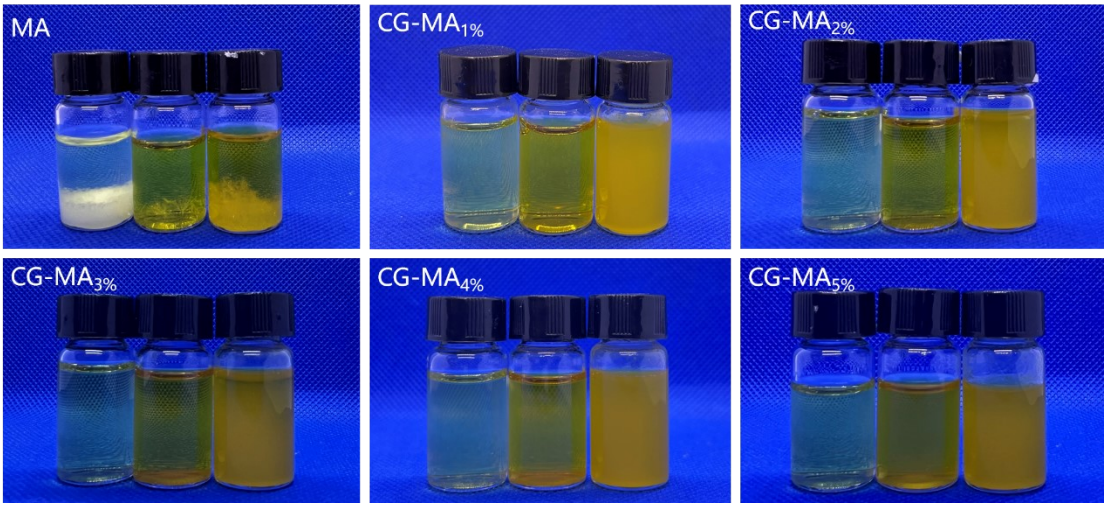

Fig. S1. Adsorption effect of CG-MA with different MA contents on $FeCl_2$ (left), $FeCl_3$ (middle), and $FeCl_{3/2}$ (right).

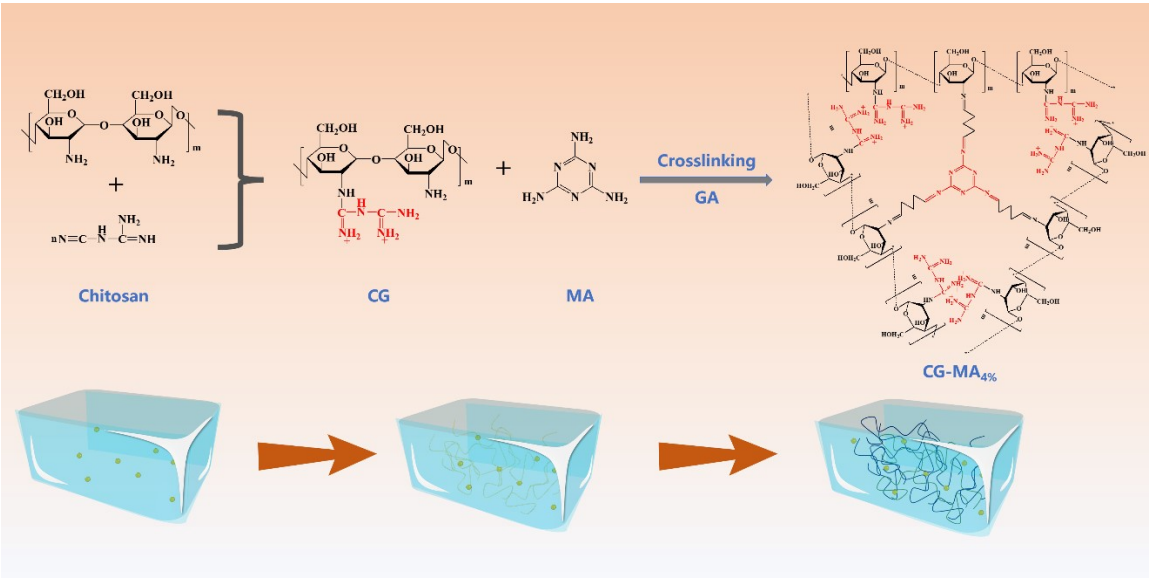

Fig. S2. Schematic illustration of design, optimization and fabrication of adsorbable ionic gel.

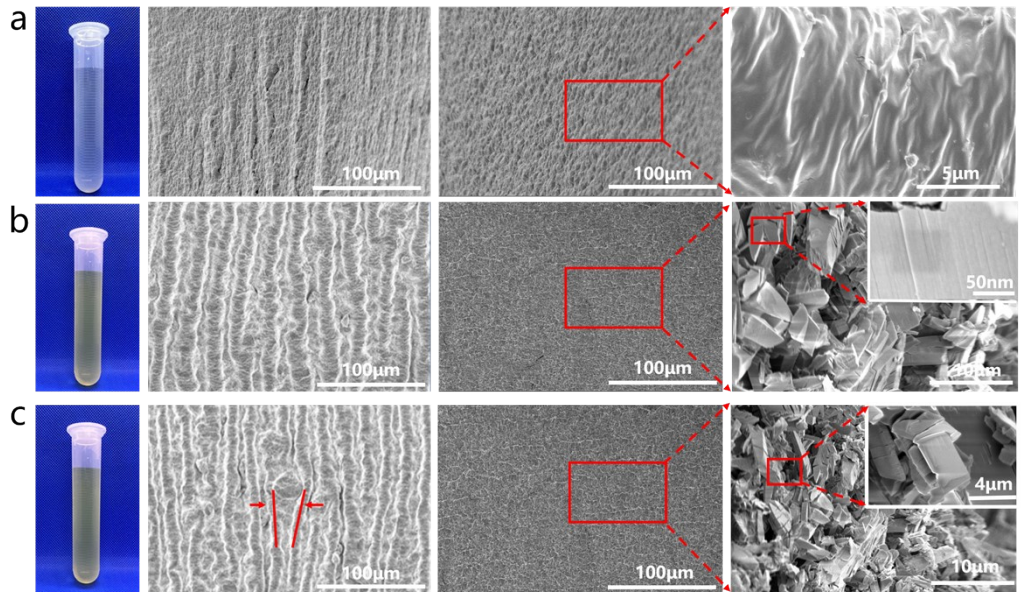

Fig. S3. Visual appearance and SEM images of (a) chitosan, (b) CG-$MA_{4\%}$, and (c) CG-$MA_{5\%}$ ionic gels.

Fig. S3 shows the surface morphology of the ionic gels obtained by the casting method for chitosan, CG-$MA_{4\%}$, and CG-$MA_{5\%}$. As can be seen from the figures, both the chitosan film and CG-$MA_{4\%}$ showed a uniform and dense morphological structure with no obvious pores appearing. As shown in **Fig. S3a**, the surface of pure chitosan film was more uniform, and no obvious fold traces were seen although cross-linking reaction occurred under the action of glutaraldehyde. By contrast, when MA was introduced, the surface of the membrane showed obvious folds and wrinkles (**Fig. S3b**), indicating that MA was cross-linked in the membrane interior. It was also observed from the cross-section that the cross-linking reaction became more and more complete with the increase of MA content, resulting in tighter structure of the membrane. Further increasing the MA content to 5% (**Fig. S3c**), the seam of the folds was observed to be much smaller and tighter, even adhesion among folds occurred. This resulted in the formation of a closely-packed mesh structure inside the membrane, which compressed the migratory channels of Cl^- ions and limited the thermodiffusion of Cl^-.

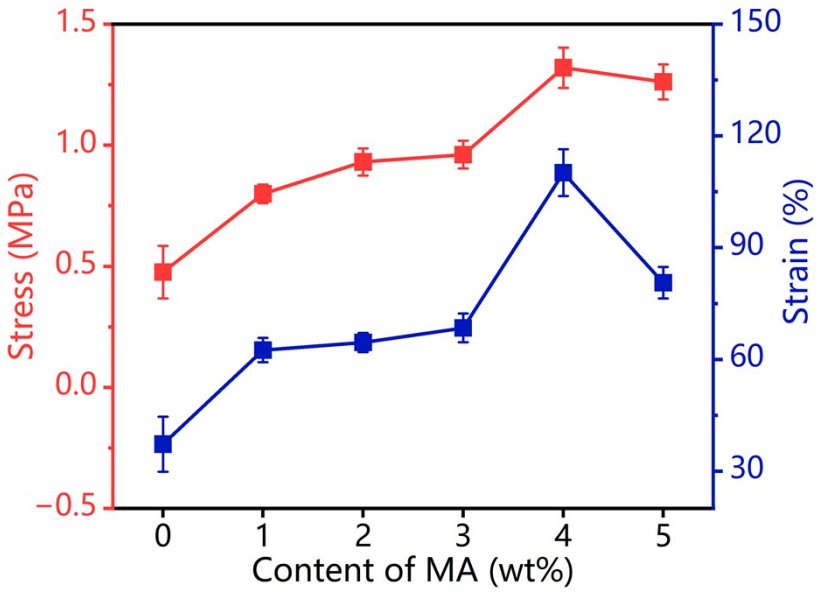

Fig. S4. Effect of MA content on the mechanical performances of CG-$MA_{4\%}$ ionic gel after immersion in electrolyte.

As shown in **Fig. S4**, addition of MA significantly improved the tensile strength of CG-$MA_{0\text{-}5\%}$ up to 1.27 MPa. This is because the triazine ring structure in molecular structure of melamine can cross-link with multiple CG macromolecules, which resulted in the formation of a denser spatial network structure and increase of the intermolecular force, thus leading to increase of the tensile strength. However, when the melamine content was 5%, the mechanical properties of the samples decreased. This was likely due to that adding more MA could result in more intramolecular cross-linking points, which eventually led to closely packed polymer mesh structure, that is, resulting in the molecular chains were difficulty of bending. Thus, the fusion of the membrane becomes brittle, affecting the mechanical properties of the membrane.

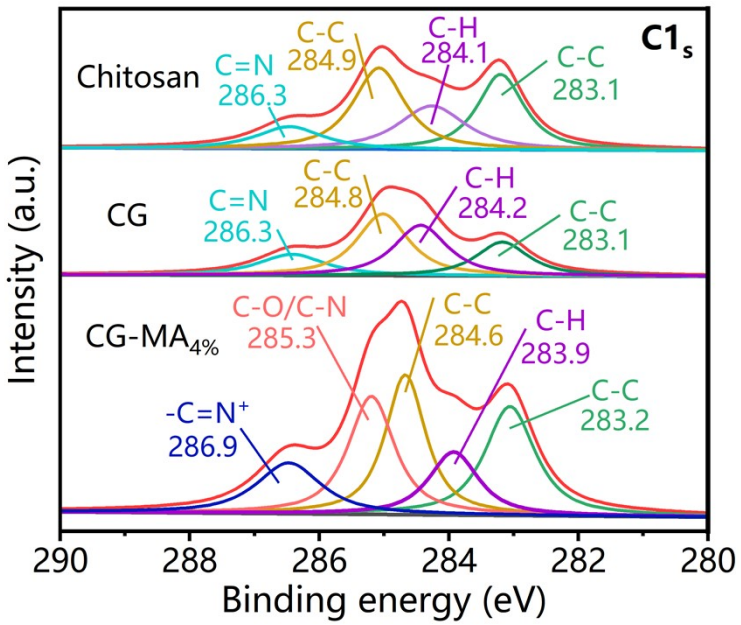

Fig. S5. C 1s XPS spectra of Chitosan, CG, and CG-$MA_{4\%}$ ionic gels.[4]

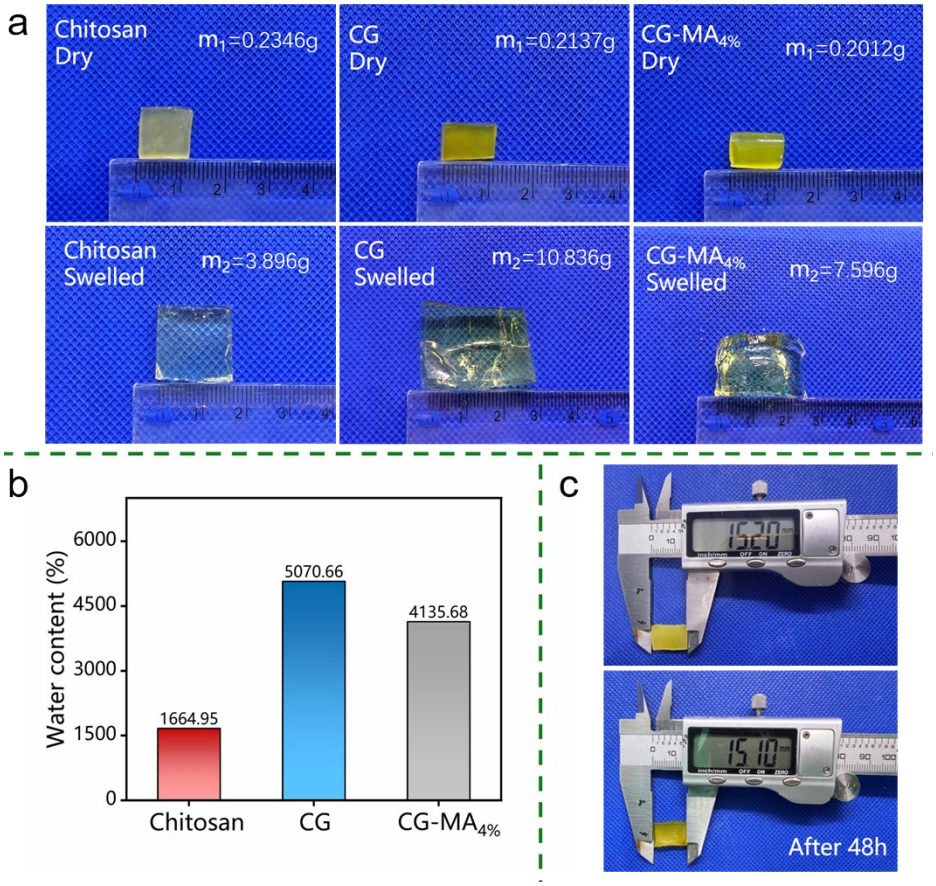

Fig. S6. Swelling of ionic gels immersed in water and electrolyte solutions. (a) Comparison of volume and weight of chitosan, CG and CG-$MA_{4\%}$ ionic gels before and after water absorption by immersion in pure water. (b) The moisture content of chitosan, CG, and CG-$MA_{4\%}$. (c) Swelling of CG-$MA_{4\%}$ ionic gel after immersion in electrolyte solution for 48 h.

Fig. S6a and **S6b** showed that CG and CG-$MA_{4\%}$ had higher absorption and swelling capacities than chitosan in pure water, with absorption rates of 5070.66 and 4135.68%, respectively. On the other hand, it is obvious that the CG-$MA_{4\%}$ ionic gel immersed in the electrolyte solution did not undergo significant swelling change (**Fig. S6c**). This implies the excellent dimensional stability of CG-$MA_{4\%}$ ionic gel after immersion in electrolyte, which can be attributed to the fact that introduction of MA can effectively inhibit swelling of the membrane and maintain the dimensional its stability.

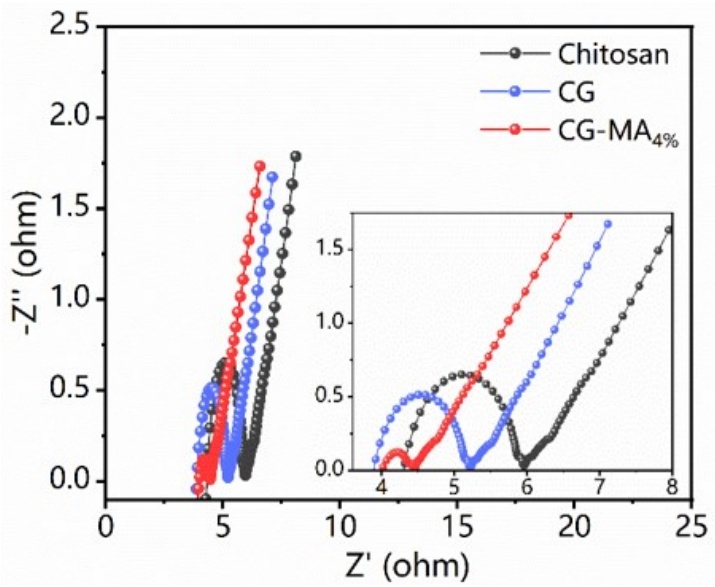

Fig. S7. Nyquist plots of chitosan, CG and CG-$MA_{4\%}$ ionic gels. The inserted image indicates the amplification in the low impedance range. The ionic conductivity was calculated by the real part of the impedance in the Nyquist plot of electrochemical impedance spectroscopy.

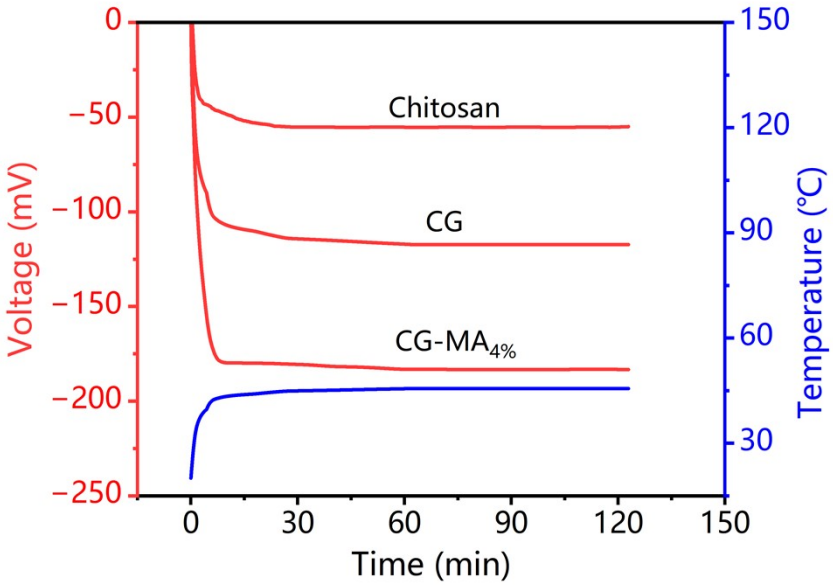

Fig. S8. Recorded open-circuit voltages and hot electrode temperatures over time for chitosan, CG, and CG-$MA_{4\%}$ ion gels. The cold electrode was fixed at 20 $^{\circ}C$ and the hot electrode was slowly warmed to 45 $^{\circ}C$ and maintained at that temperature.

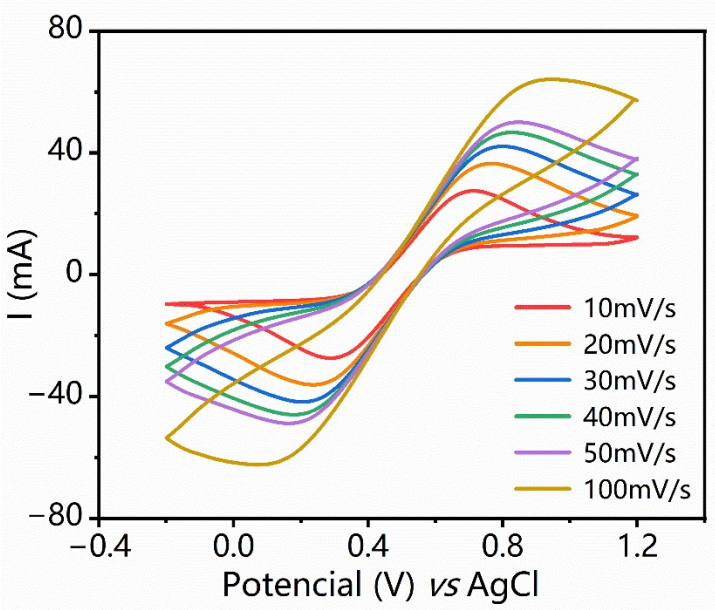

Fig. S9. Cyclic voltammetry (CV) curves of CG-$MA_{4\%}$ at different scan rates.

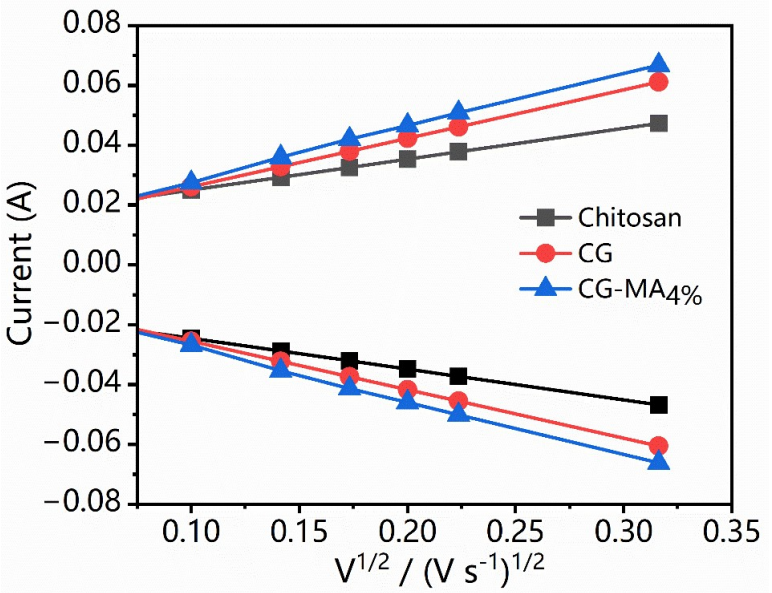

Fig. S10. Linearity of peak electrochemical activity current versus square root of scan rate for chitosan, CG and CG-$MA_{4\%}$ gel electrolytes (10-100 mV s^{-1}).

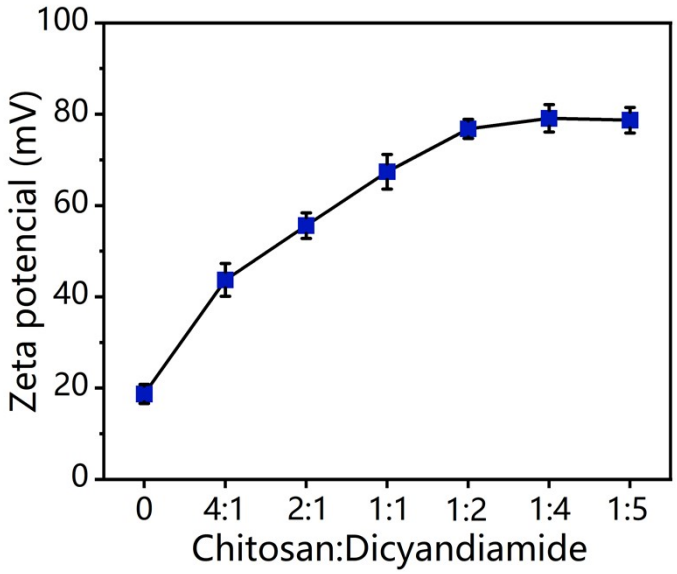

Fig. S11. Zeta potential of ionic gels with varying chitosan-to-dicyandiamide ratio.

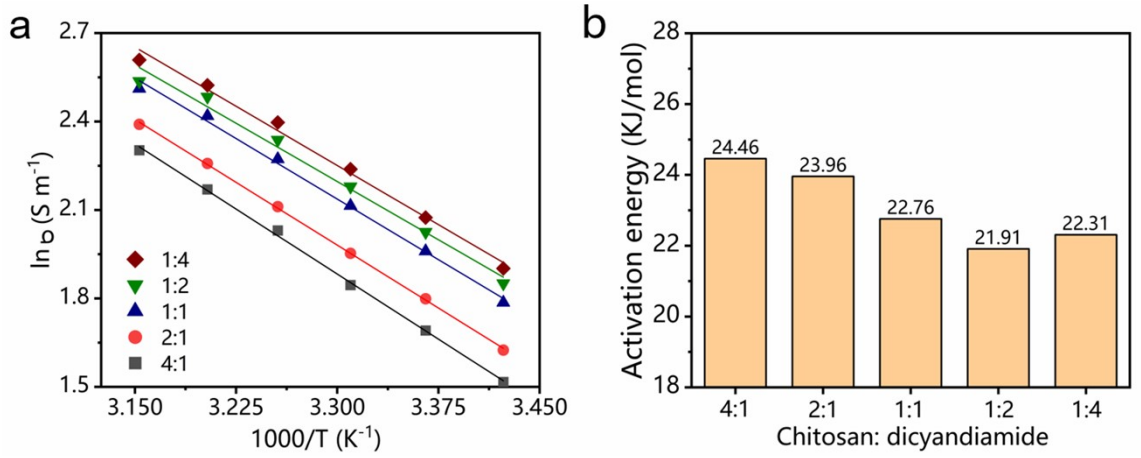

Fig. S12. Effect of chitosan-to-dicyandiamide ratio on the activation energy of ionic migration. (a) Relationship between $ln\sigma$ and $1000/T$ at different chitosan-to-dicyandiamide ratios under different temperatures. (b) Effect of dicyandiamide content on the activation energy of ion migration.

We tested the ionic conductivity of CG gels with different chitosan-to-dicyandiamide ratios under different temperatures. The ionic conductivity-temperature relationship was fitted by the Arrhenius equation, and the activation energy of the CG gels for ionic conductivity was calculated from the Eq. S17:

$$\sigma = Aexp\left(\frac{-Ea}{RT}\right) \quad (S17)$$

where A is finger front factor, E_a is ionic conduction activation energy (KJ mol^{-1}), R is gas constant (8.314 J K^{-1} mol^{-1}), and T is thermodynamic temperature (K). The relationship between $ln\sigma$ and $1000/T$ exhibits a linear relationship (**Fig. S12a**), with which the ionic conduction activation energy of CG ionic gels can be obtained from the Arrhenius equation:

$$Ea = -b \times R \quad \text{S18}$$

where b is slope of the curve of $ln\sigma$ (S cm^{-1}) vs. $1000/T$ (K^{-1}). As shown in **Fig. S12b**, the activation energy for ionic conductivity of the CG ionic gels at the chitosan-to-dicyandiamide ratio of 4:1, 2:1, 1:1, 1:2 and 1:4 was calculated to be 24.46, 23.96, 22.76, 21.91, and 22.31 KJ mol^{-1}, respectively. The activation energy of the CG gel for ionic conductivity gradually decreased as increasing the N^+ groups, reaching the lowest activation energy at chitosan-to-dicyandiamide of 1:2, which is consistent with the results of the thermopower. The migration activation energy of the gel was reduced by introduction of dicyandiamide, which was attributed to that each dicyandiamide group provided two N^+ adsorption sites, resulting in increase in the density of the distribution of adsorption sites for C^- ions and a reduction in the migration resistance. On the other hand, with introduction of more dicyandiamide, the dual N^+ groups could trap Cl^- ions and inhibit their migration, leading to increase in migration activation energy (**Fig. S12b**).

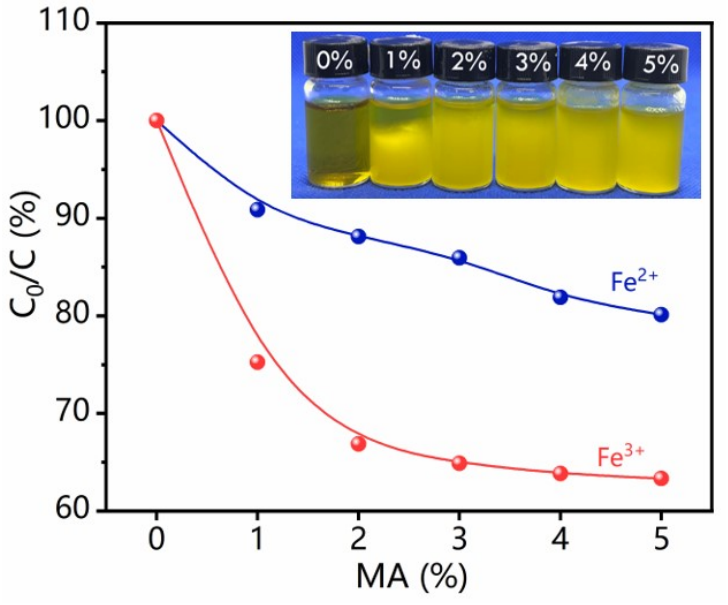

Fig. S13. Relative concentration changes of the redox couple in the soaking solution with different MA contents.

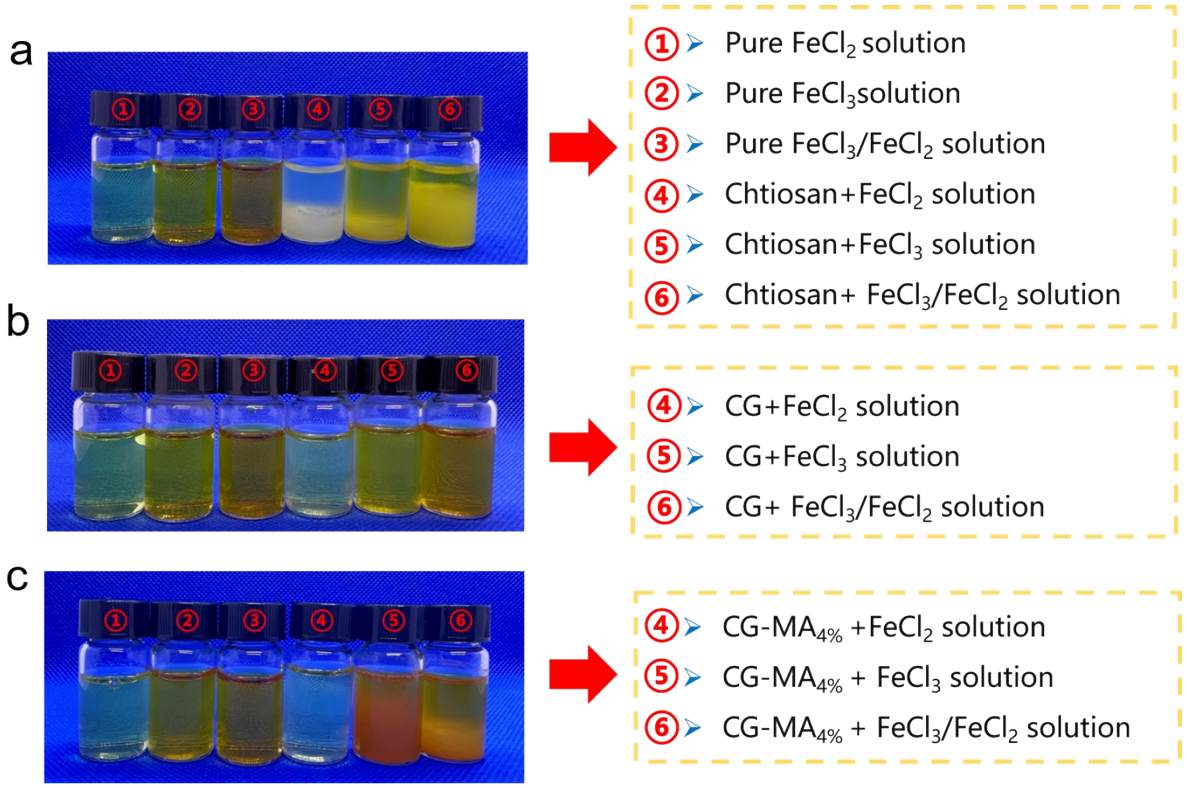

Fig. S14. Adsorption of the soaking solution ($FeCl_2$, $FeCl_3$, and $FeCl_{3/2}$) with (a) chitosan gel, (b) CG gel, and (c) CG-$MA_{4\%}$ gel.

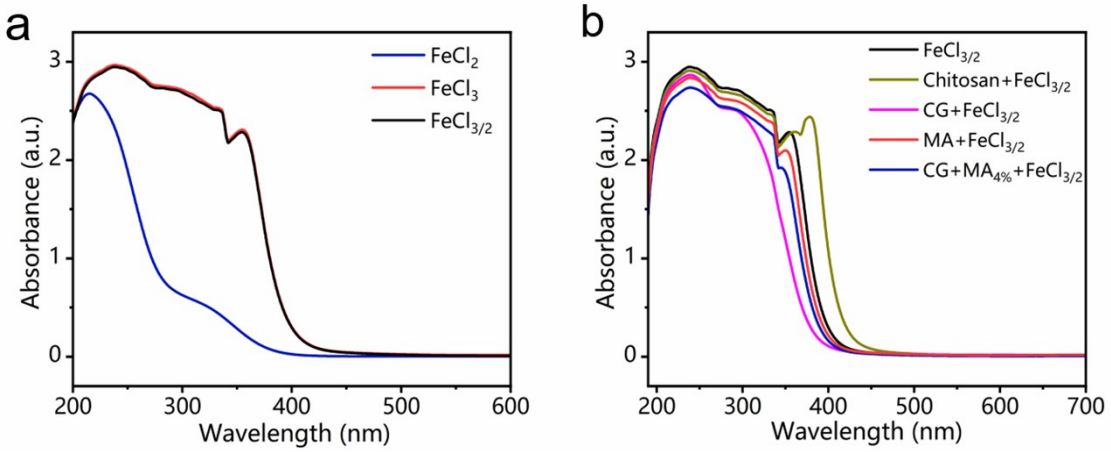

Fig. S15. UV-vis absorption spectra corresponding to (a) $FeCl_2$, $FeCl_3$, and $FeCl_3/FeCl_2$ and (b) different combinations of gels and $FeCl_{3/2}$ solutions.

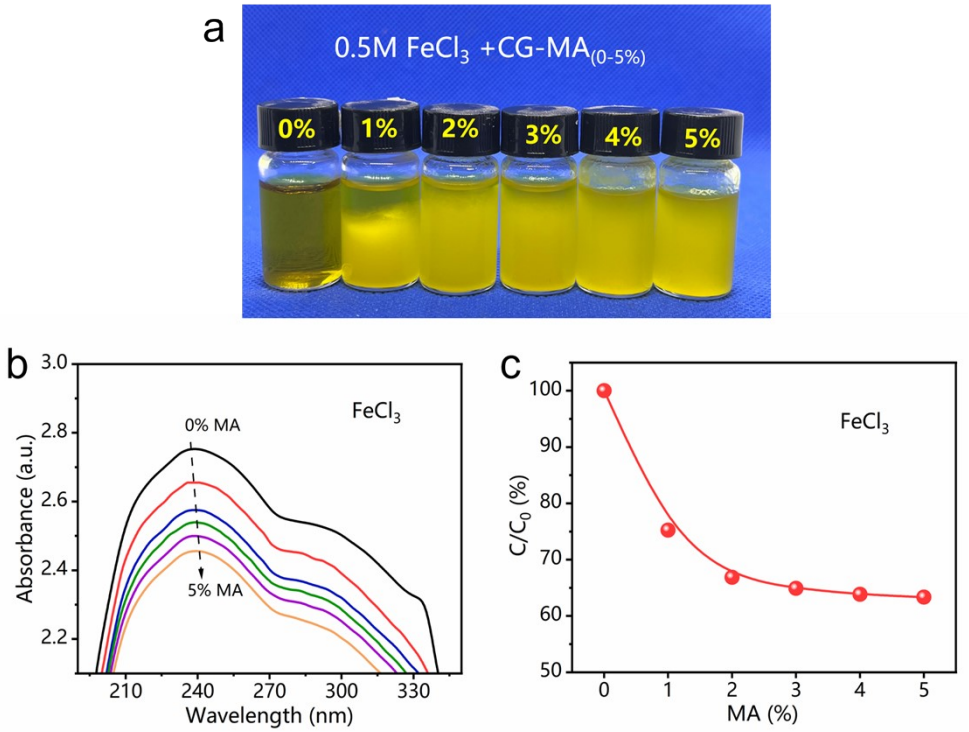

Fig. S16. (a) Visual appearance, (b) UV-vis absorbance spectra, and (c) relative concentration changes of $FeCl_3$ in solutions containing 0.5 M $FeCl_3$ and $CG\text{-}MA_{(0\text{-}5\%)}$.

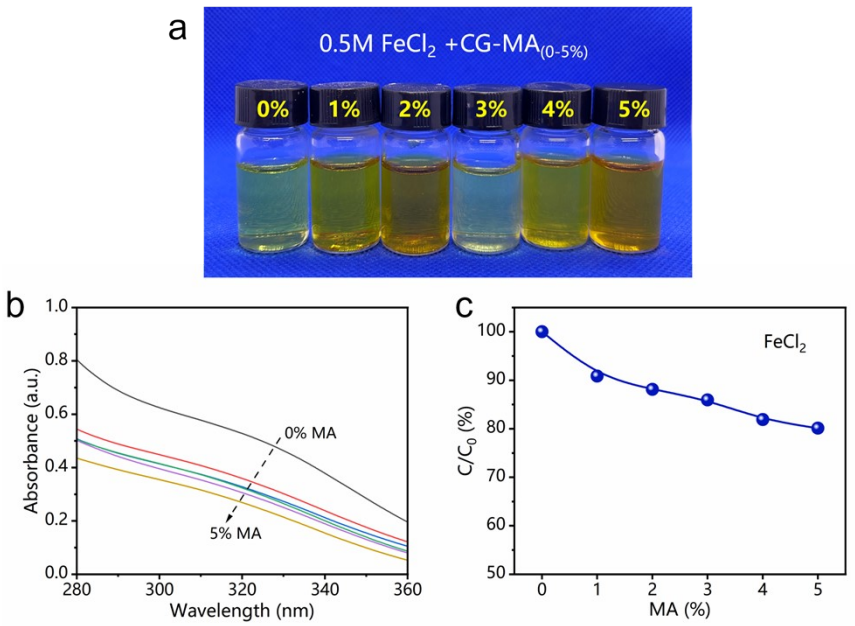

Fig. S17. (a) Visual appearance, (b) UV-vis absorbance spectra, and (c) relative concentration changes of $FeCl_2$ in solutions containing 0.5 M $FeCl_2$ and $CG\text{-}MA_{(0\text{-}5\%)}$.

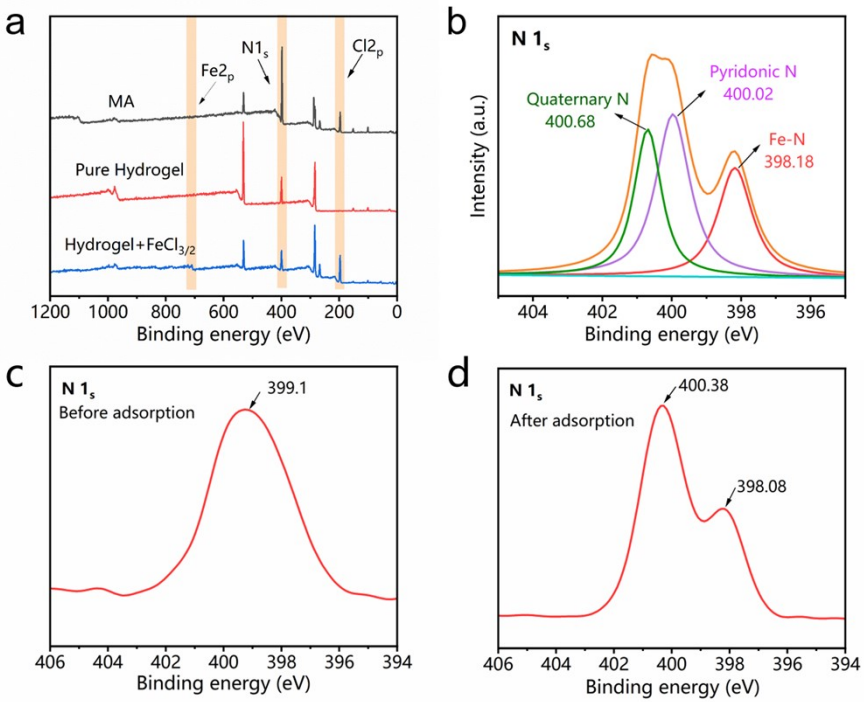

Fig. S18. (a) XPS patterns of MA, pure ionic gels, and dried precipitates. (b) The N1s peak splitting spectrum. (c) N1s characteristic peaks of $CG\text{-}MA_{4\%}$ gels. (d) N1s characteristic peak of $CG\text{-}MA_{4\%}$ gel after adsorption.[5]

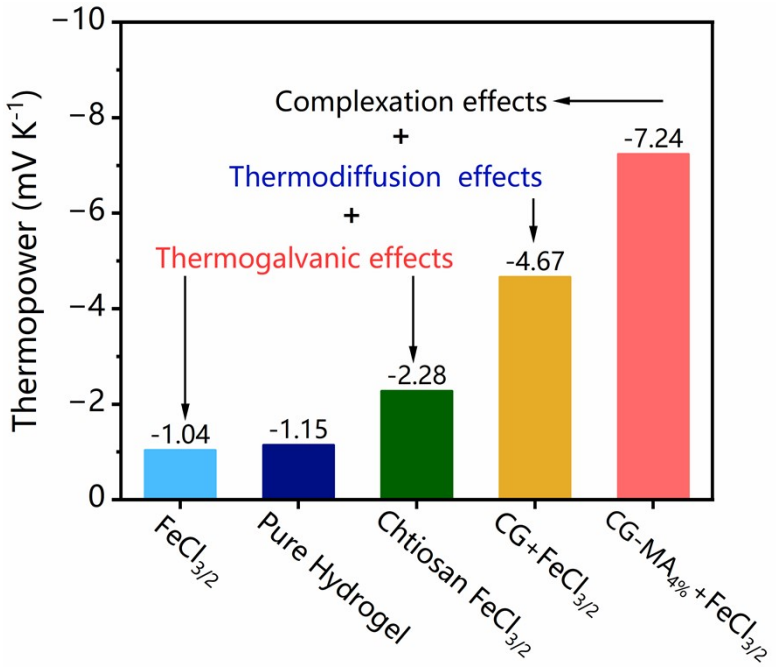

Fig. S19. The thermopower variation of different ionic gel components, including pure $FeCl_3/FeCl_2$ electrolyte solution and CG-$MA_{4\%}$ ionic gel, as well as chitosan, CG, and CG-$MA_{4\%}$ ionic gels after immersion in electrolyte solution.

As shown in **Fig. S19**, the thermopower of pure $FeCl_{3/2}$ electrolyte solution (-1.04 mV K^{-1}) is provided by the thermogalvanic effects. The thermopower of the pure hydrogel (-1.15 mV K^{-1}) is provided by the thermodiffusion effects of the OH^- free from the internal water molecules. The thermopower of chitosan-$FeCl_{3/2}$ (-2.28 mV K^{-1}) is caused by the enhanced thermogalvanic effects due to complexation of chitosan on metal ions. The thermopower of CG-$FeCl_{3/2}$ is -4.67 mV K^{-1}, which was firstly provided by the thermogalvanic effect of the $FeCl_3/FeCl_2$ redox electrolyte and secondly caused by introduction of positively charged amino groups to enhance the thermodiffusion effect. Moreover, the thermopower of CG-$FeCl_3$ and CG-$FeCl_2$ were -3.12 and -2.72 mV K^{-1}, respectively, which were all contributed entirely by the thermodiffusion effect (combined thermodiffusion of Cl^- and CG gels itself). Thus, for CG-$FeCl_{3/2}$, the thermodiffusion effect contributed to 66.8% at most (-3.12 mV K^{-1}), and the

thermogalvanic effect contributed to 33.2% (-1.55 mV K^{-1}). These results indicate that the thermodiffusion effect could be significantly enhanced by introduction of dicyandiamide. The thermopower of -7.24 mV K^{-1} the CG-$MA_{4\%}$ is provided by a combination of thermodiffusion effects and thermogalvanic effects enhanced by the adsorption of metal ions by the chitosan hydrogel after the introduction of melamine.

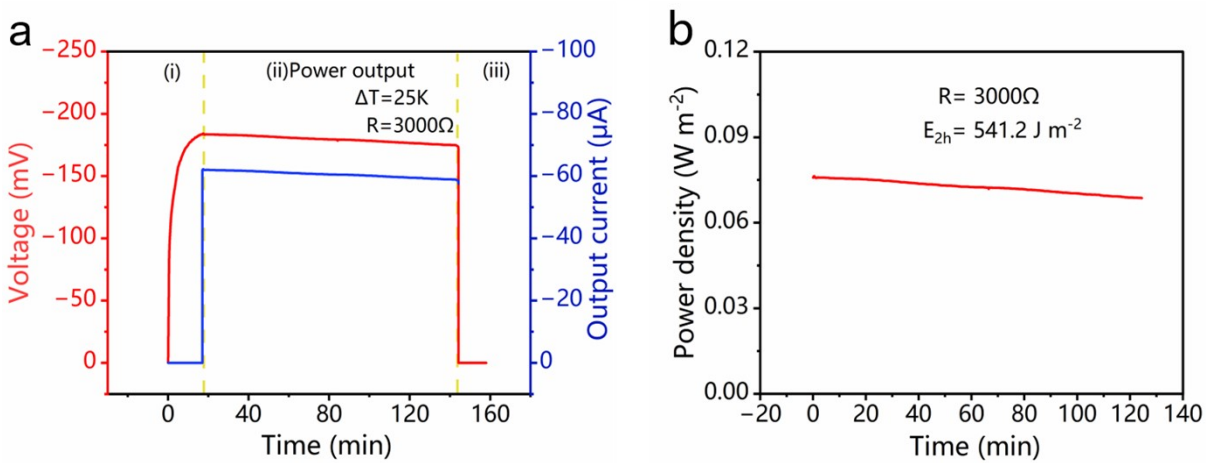

Fig. S20. Energy output of ITEC with large external resistor. (a) Voltage and current curves of three working stages under an external resistance of 3000 Ω. (b) The output power density of stage ii at 3000 Ω external resistance for 120 min.

The voltage and current curves for three operating phases under 3000 Ω external resistance were measured. The output power density of stage ii at 3000 Ω external resistance for 120 min is shown in **Fig. S20a**, and the energy density (E_{2h}) of ITEC was finally calculated to be 541.2 J m^{-2} (**Fig. S20b**), indicating excellent output performance of the ITEC even under high external load resistance.

The selection of a small resistor in this study can be explained by Ohm's law for closed circuits, and the power output of the power supply can be determined from the Eq. (S19):

$$P = I^2R = (\frac{E}{R+r})^2R = \frac{E^2R}{(R-r)^2+4Rr^2} \quad (S19)$$

where E is the supply electromotive force, R is the external load resistance, and r is the internal resistance of the supply. Accordingly, when the external load resistance is close to the internal resistance, the output power is maximized. With the EIS technology analysis, we confirmed that the resistance of CG-$MA_{4\%}$ ionic gel was small. Therefore, we chose to connect a small external load resistance (20 Ω) to maximize the output power for higher energy density.

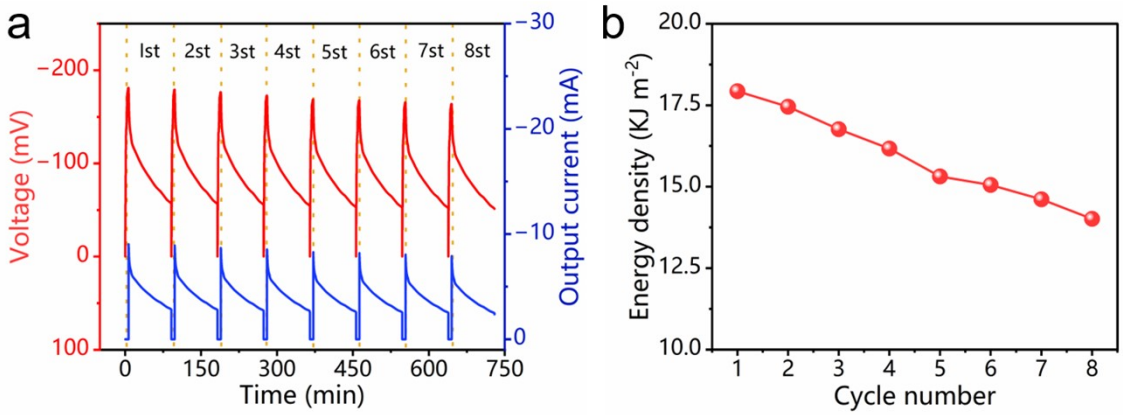

Fig. S21. Cyclic stability over eight cycles of quasi-continuous charging and discharging. (a) Voltage and current profile changes during eight cycles of internal load discharge. (b) Energy output E_{90min} for eight cycles.

We repeated charging and discharging for eight cycles consecutively with an external 20 Ω load resistor after thermal charging at a temperature difference of 25 degrees. As shown in **Fig. S21**, a total energy density of 127.29 KJ m^{-2} was harvested from the eight cycles, which corresponded to an average E_{90min} of 15.91 KJ m^{-2} for each cycle.

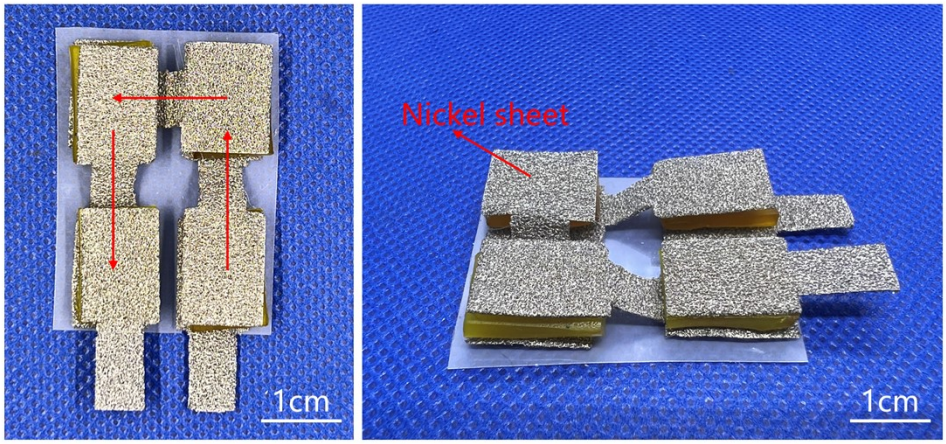

Fig. S22. Images of 4 ITECs connected in series to form an integrated device.

Supplementary table

Table. S1 Comparison of thermoelectric properties of the CG-$MA_{4\%}$ with reported ionic gel devices

Matrix materials	Thermopower (mV K^{-1})	σ (mS cm^{-1})	Power Density (W m^{-2})	Refs.
PAM/CMC/Li2SO4/$Fe(CN)_6^{4-/3-}$	11.58	18.4	0.0152	Ref.[6]
PAM/CMC/$Fe(CN)_6^{4-/3-}$	3.63	9.4 (25°C)		Ref.[6]
PVA/$Fe(CN)_6^{4-/3-}$	1.42	0.62	0.32	Ref.[7]
PAAm/$Fe(ClO_4)^{3-}$/$Fe(ClO_4)^{2-}$	1.46	65.32	0.043	Ref.[8]
PVA/$Fe^{3+/2+}$	-1.02	10.6	$2.5*10^{-3}$	Ref.[9]
PVA/$Fe(CN)_6^{4-/3-}$	1.21	6.3	$2.5*10^{-3}$	
BC/NaCl	27.3	204.2		Ref. [10]
PNIPAM/I^-/I^{3-}	0.71/-1.91	1	1	Ref. [3]
Li_2SO_4/PAAm/CA	11.5		0.09438	Ref.[11]
AMPS/$Fe(CN)_6^{4-/3-}$	1.6		0.976	Ref.[12]
Cellulose/$BzMe_{3/4}NOH$	2.61		0.42	Ref.[13]
PVA/$Fe(CN)_6^{4-/3-}$	6.5		1.77	Ref.[14]
Chitosan/$Fe^{3+/2+}$	-7.24	127.8	4.52	This work

Reference

1. C. G. Han, X. Qian, Q. K. Li, B. Deng, Y. B. Zhu, Z. J. Han, W. Q. Zhang, W. C. Wang, S. P. Feng, G. Chen and W. S. Liu, *Science*, 2020, **368**, 1091-1096.
2. J. Liu, W. Zeng and X. M. Tao, *Adv. Funct. Mater.*, 2022, **32**, 2201021.
3. J. J. Duan, B. Y. Yu, K. Liu, J. Li, P. H. Yang, W. K. Xie, G. B. Xue, R. Liu, H. Wang and J. Zhou, *Nano Energy*, 2019, **57**, 473-479.
4. S. J. Yuan, P. Zhang, Z. Y. Yang, L. Lv, S. W. Tang and B. Liang, *Int. J. Biol. Macromol,* 2018, **109**, 287-302.
5. T. Yamashita and P. Hayes, *Appl. Surf. Sci.*, 2009, **255**, 8194-8194.
6. Z. Q. Zhou, Y. F. Wan, J. Y. Zi, G. M. Ye, T. S. Jin, X. M. Geng, W. B. Zhuang and P. Yang, *Mater. Today Sustain.*, 2023, **21**, 100293.
7. Z. Y. Lei, W. Gao, W. Y. Zhu and P. Y. Wu, *Adv. Funct. Mater.*, 2022, **32**, 2107105.
8. C. Xu, Y. Sun, J. J. Zhang, W. Xu and H. Tian, *Adv. Energy Mater.*, 2022, **12**, 2200858.
9. P. H. Yang, K. Liu, Q. Chen, X. B. Mo, Y. S. Zhou, S. Li, G. Feng and J. Zhou, *Angew. Chem. Int. Ed.*, 2016, **55**, 12050-12053.
10. Z. T. Wu, B. X. Wang, J. Li, R. L. Wu, M. T. Jin, H. W. Zhao and S. Y. Chen, *Nano Lett.*, 2022, **22**, 8152-8160.
11. J. H. Chen, L. Zhang, Y. Y. Tu, Q. Zhang, F. Peng, W. Zeng, M. Q. Zhang and X. M. Tao, *Nano Energy*, 2021, **88**, 8152.
12. Z. Y. Lei, W. Gao and P. Y. Wu, *Joule*, 2021, **5**, 2211-2222.
13. Y. Hu, M. Z. Chen, C. R. Qin, J. P. Zhang and A. Lu, *Carbohydr. Polym.*, 2022, **292**, 119650.
14. L. Liu, D. Zhang, P. Bai, Y. Mao, Q. Li, J. Guo, Y. Fang and R. Ma, *Adv. Mater.*, 2023, **35**, 2300696.